Received 20 March 2023; revised 24 May 2023; accepted 31 May 2023. Date of publication 8 June 2023; date of current version 22 June 2023.

Digital Object Identifier 10.1109/OJAP.2023.3283994

Post-Fabrication Technique to Manage Material Variations in 3-D Printed Microstrip Antenna Substrates

ZERE IMAN, ZUBAIR AKHTER (Member, IEEE), YIYANG YU (Graduate Student Member, IEEE), AND ATIF SHAMIM (Senior Member, IEEE)

Computer, Electrical, and Mathematical Sciences and Engineering (CEMSE) Division, King Abdullah University of Science and Technology, Thuwal 23955, Saudi Arabia

CORRESPONDING AUTHOR: Z. IMAN (e-mail: zere.iman@kaust.edu.sa)

This work was supported by the CEMSE Division at King Abdullah University of Scienceand Technology, Kingdom of Saudi Arabia under Grant BAS/1622/01-01.

ABSTRACT To fulfill the growing demand of next-generation wireless devices, additive manufacturing has emerged as the most economical, environmentally friendly, and high-throughput technique for mass manufacturing. At present, however, 3D-printed antenna substrates show 4%–8% variation in relative permittivity (ε_r) compared with typical tolerance values of less than 2% in commercially available substrates. This relatively large tolerance in 3D-printed substrates is attributed to the variations in the quality of the material cassette, extrusion speed, temperature profile, individual layer thickness, printing orientation, infill patterns, and density (i.e., air gaps). Consequently, the resonant frequency (f_r) of antennas on 3D-printed substrates may vary batch-to-batch; this is a major issue for narrow band antennas such as microstrip antennas. This study presents a post-fabrication technique capable of compensating for variations in the ε_r of 3D printed substrates, focusing on microstrip patch antennas (MPAs). The proposed technique, suitable for correcting the f_r of a single microstrip patch antenna, uses either a single blind via or an array of vias in the 3D-printed substrate. The direction and shift in f_r depend on the location and dimensions of the via. Through electromagnetic simulations, a complete set of guidelines has been provided for selecting the number of vias, their locations, and their dimensions for a desired amount of shift in the f_r of the antennas. Furthermore, the shift of the f_r is explained using a proposed improvised transmission-line model of the MPA (incorporating vias). To confirm the proposed technique, two MPAs were fabricated on a 3D-printed substrate and it is shown that their f_r values can be shifted upward or downward by following the proposed guidelines. The maximum shift in f_r, without significantly affecting MPA performance, can reach up to 13%, which is sufficient to manage variations in ε_r values of 4%–8%.

INDEX TERMS 3D printing, electrical permittivity, frequency tuning, microstrip patch antenna, post-fabrication technique.

I. INTRODUCTION

ADDITIVE manufacturing (AM) has emerged as a mainstream fabrication technology for wearables, medical devices, and automotive systems owing to its suitability during high-throughput mass manufacturing [1]. Because of the speed of printing, diversity of printed materials, low cost, reduced material wastage, and ability to develop complex geometries, 3D printing is becoming a preferred fabrication technique and is replacing conventional subtractive techniques, such as lithography and micromachining. In addition to its utility in various fields, a wide range of radio frequency (RF) components, such as antennas [2], [3], [4], [5], [6], [7], [8], [9], [10], [11], [12], absorbers [13], [14], couplers [15], filters [16], frequency-selective surfaces [17], diplexers [18], lenses [19], [20], [21], and waveguides [22], have been produced using 3D printing approaches.

Although 3D printing has many clear advantages, the homogeneity and consistency in the electrical properties of produced components depends on multiple factors, including the quality of the material cassette, extrusion speed, temperature profile, individual layer thickness, print orientation, infill patterns, and density (i.e., air gaps) [23]. Previous

research [24], [25], [26], [27] has reported that the ε_r of the 3D printed substrates varies with infill ratio. Reference [28] has reported that practical 3D printed substrates are neither isotropic or homogeneous. Variations of 4%–8% in ε_r of 3D-printed substrates can lead to the undesirable alteration of important parameters, such as phase velocity and characteristic impedance, which ultimately have a negative influence on the performance of the radio frequency (RF) component. However, the variation of ε_r in standard microwave substrates is typically <2.0% [29], [30]. Such large deviations in the ε_r of 3D-printed substrates presents a major issue for narrowband microwave components and systems, particularly antennas. Deviations in substrate ε_r can result in antennas exhibiting f_r values that differ from the designed or simulated value. One possible solution to correct for this error is to redesign and refabricate the sample with a corrected ε_r value that will result in updated antenna dimensions. However, the second round of design (EM simulations to identify new dimensions) and re-fabrication adds to the overall cost and is not an environmentally friendly solution. However, efficient post-fabrication techniques can be developed to correct for shifts in f_r without the requirement for additional rounds of design and fabrication cycles.

As mentioned previously, the f_r deviation is critical for narrowband antennas, such as MPA. Many techniques reported in the literature allow for the adjustment or reconfiguration of f_r of the MPA, such as varactors [31], fluids and liquid crystals [32], [33], low temperature cofired ceramic (LTCC) substrates [34], [35], and an anisotropic artificial dielectric layer (AADL) [36]. However, 1) most of these approaches are not used during post-fabrication correction, and 2) most are limited to inducing a frequency shift in one direction (downwards). Furthermore, there are currently no precise guidelines on how these corrections can be applied to achieve the desired frequency shift. Previous research [37] presented a post-fabrication technique capable of tuning the frequency of the MPA using an air pocket beneath the substrate layer; however, this technique is difficult to apply with 3D-printed substrates because milling away large section of the substrate can damage the layers of the conductor because they are less rigid than those of conventional RF substrates.

In this study, we propose a new way by which the f_r of the single 3D-printed antenna may be corrected through a single blind via or an array of vias on originally fabricated samples without the requirement to produce another sample. A small number of previous studies [38], [39] demonstrated the utility of vias for tuning the frequency of MPAs, achieving miniaturization [40] and bandwidth enhancement [41]. In 1980, Schaubert et al. [38] demonstrated that antenna f_r can be modified by placing two shorted vias in specific locations. The f_r of MPAs with shorted vias has been subsequently calculated using transmission-line models in [42], [43], [44] and with cavity models in [45]. The latter requires complicated analysis, including a full modal expansion of the cavity fields. Moreover, shorted vias have been utilized to control frequency separation between the TM_{01} and TM_{03} modes of rectangular MPAs [46]. In summary, techniques depending on the use of shorted vias for tuning are limited to shifting the fundamental f_r to a higher frequency. Furthermore, variations in the 3D-printed substrate may require the antenna to be tuned in either direction, i.e., downwards and upwards. In our proposed technique, which is based on blind vias, the frequency can be shifted in both directions by optimizing both the via location and dimensions of the via. We demonstrated that f_r can be shifted by up to 13% without significantly affecting MPA performance. This is sufficient to cater for variations of 4%–8% in the ε_r values of 3D-printed antenna substrates. Finally, a complete set of guidelines are provided to enable effective use of this technique to achieve the desired f_r.

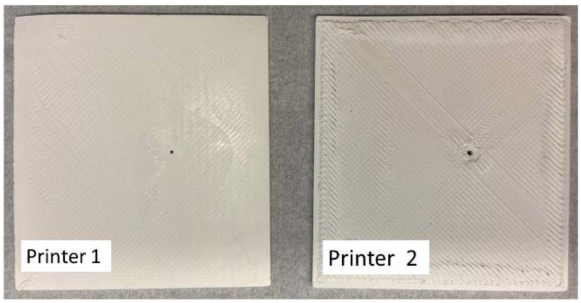

FIGURE 1. Printed samples for material characterization.

This study is structured as follows. Section II defines the scope of the problem and demonstrates the necessity of the proposed technique by showing permittivity variations in 3D-printed materials at 1 and 7.5 GHz. Section III describes how the operational f_r of the 3D-printed patch antenna can be shifted to lower or higher frequencies and presents complete guidelines to move the resonance position in the desired direction. Section IV validates the proposed technique, and Section V presents the conclusion of this paper.

II. PERMITTIVITY VARIATION IN 3D PRINTED MATERIALS

In this section, we aim to quantify variations in ε_r for 3D-printed substrates. Fourteen dielectric substrates with a length of 56 mm, a width of 50 mm, and a height of 1.5 mm were printed in 3D using two commercial printers, hereafter abbreviated as 1 (Ultimaker) [47] and 2 (Creator Pro) [48], using an ABS filament with an ε_r of 3 and measured tangent loss of 0.046. The substrates have been printed with the best possible settings, i.e., the infill ratio of both printers have been set to 100%. Fig. 1 shows two such printed substrates. Subsequently, their ε_r was obtained using an Agilent E4991A RF Impedance Analyzer at 1 GHz. As shown in Fig. 2, for printer 1, a maximum ε_r variation of 4.48% was observed for the seven samples. The printing quality for printer 2 is worse, thus resulting in a maximum variation of 8.84%. Next, ε_r was measured at different locations of one sample printed on each commercial printer. Fig. 3 shows that ε_r varies within the sample at seven different locations; this variation is 4.39% for printer 1 and 7.61% for printer 2. To confirm that this difference did not

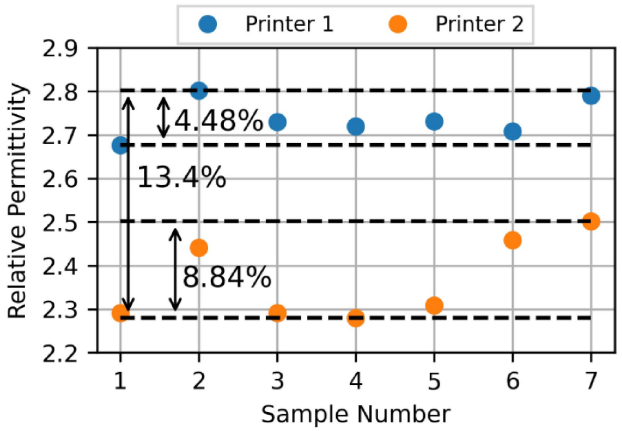

FIGURE 2. Measured relative permittivity for different samples at 1 GHz.

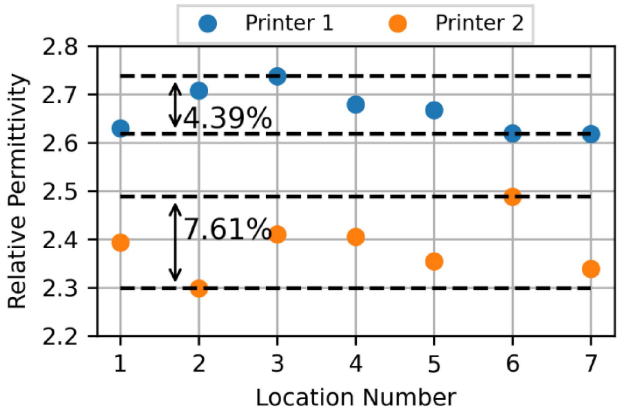

FIGURE 3. Measured relative permittivity at different locations within the sample at 1 GHz.

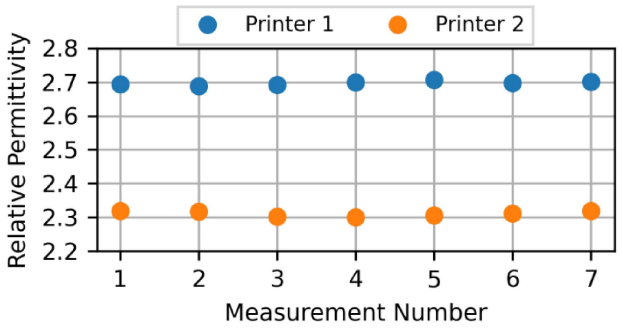

FIGURE 4. Measured relative permittivity for repeated measurements at the same location at 1 GHz.

arise from a measurement error, ε_r was measured multiple times at a specific location for each sample. The results of this verification are shown in Fig. 4; the negligible variation demonstrates that the measurement error is insignificant.

To examine the permittivity variation at a higher frequency (7.5 GHz), we 3D-printed five additional samples using a third commercial printer (Raise 3D) [49]. Five T-resonators were screen-printed on 3D-printed substrates using conductor paste DuPont PE819. The permittivity of each sample was obtained from its scattering parameters. As shown in Fig. 5, the permittivity variation is >10%, showing both that

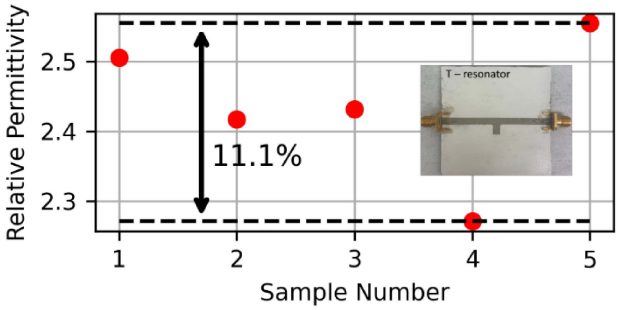

FIGURE 5. Relative permittivity variation for printed dielectric samples at 7.5 GHz.

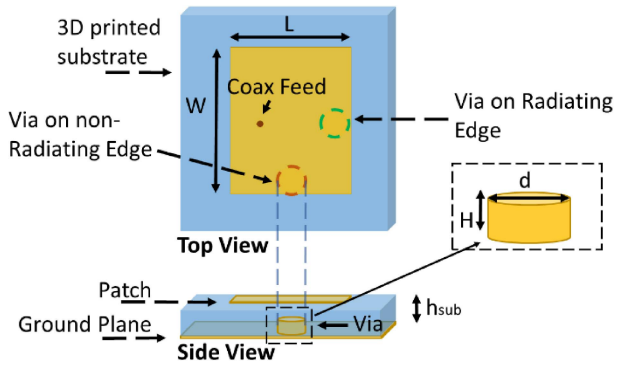

FIGURE 6. Conceptual visualization of MPA with blind vias.

considerable ε_r variation (up to 10%) exists in 3D-printed substrates and this variation changes depending upon the printer and frequency used. Consequently, there is a requirement to manage this variation, particularly for narrowband antennas.

III. POST-FABRICATION CORRECTION TECHNIQUE

Permittivity variation in 3D-printed substrates is a major issue for narrowband components such as MPA. We thus chose MPA for this study because it is among the most popular antenna by virtue of its low profile, decent gain, low cost, and ease of fabrication, as well as the ease of its integration into circuits. Fig. 6 shows top and side views of a conceptual visualization for an MPA on a 3D-printed substrate. The antenna is fed by a coaxial cable, and both the radiating (separated by length L) and non-radiating (separated by width W) edges are shown. The field components of the radiating edges add in phase contributions and provide the maximum radiation, whereas those of the non-radiating edges cancel each other out in a direction perpendicular to the ground plane [50].

As discussed in the Introduction, we here introduce a blind via or an array of blind vias to compensate for the frequency shift. For this technique, it is important to know various parameters, such as the position, dimensions, and number of blind vias. These have been examined through EM simulations in CST Microwave Design Studio (CST) and are discussed in the following sub-sections. As a reference, an antenna with substrate dimensions 56 mm $\times$ 50 mm $\times$ 1.5 mm, and patch dimensions L $=$ 27.4 mm

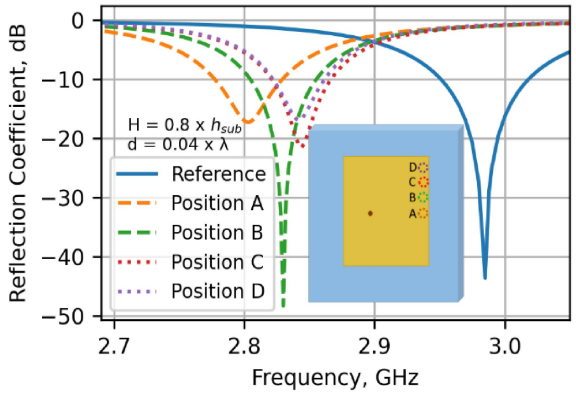

FIGURE 7. Resonant frequency shift with respect to position along radiating edge.

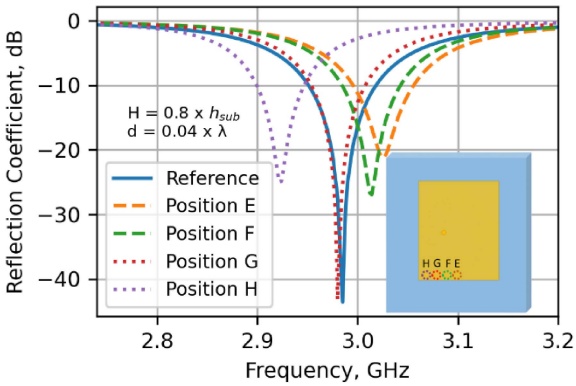

FIGURE 8. Resonant frequency shift with respect to position along the non-radiating edge.

and W = 35.33 mm has been taken. The feed location is 5.75 mm offset from the patch center. The substrate's permittivity and loss tangent are 3 and 0.0046, respectively.

A. VIA POSITION STUDY

To examine the influence of via position on f_r behavior, the blind via extending from the ground plane was inserted along both the radiating and non-radiating edges. Without this via, the MPA works at 2.985 GHz. For this study, via dimensions of diameter $d = 0.04\lambda$ (where wavelength $\lambda =$ 10.05 mm) and height $H = 0.8h_{sub}$ (where substrate height $h_{sub} = 1.5$ mm) were selected; the effect of via dimensions is considered in detail in the following subsection. For the radiating edge, we selected four positions. The position was varied from the center (Position A) to the corners of the patch (Position D) along the radiating edge, as shown in Fig. 7. If the blind via is inserted into Position A, f_r is reduced and a shift of 165 MHz is observed. If the blind via is inserted into Position B, f_r goes downwards and a shift of 155 MHz is observed. Generally, the amount of shift decreases from Position A to Position D as the blind via moves closer to the corner of the patch. The central position (Position A) provides the maximum downward shift. Note that if the via is placed along the other radiating edge (i.e., that closer to the coaxial cable), the results slightly differ because of the close proximity of the feed. The downward shift can be explained as follows. The current is at a minimum while the voltage is at a maximum at the radiating edges. Thus, this via introduces a significant capacitance, which is responsible for lowering f_r. It is worth mentioning that the via insertion in this position influences the matching of the antenna since capacitance are added at the critical point of MPA. However, the reflection coefficient is within the acceptable limit of –10 dB.

To explore the mechanisms by which the via influences f_r when it was placed along the non-radiating edge, a blind via of height $H = 0.8h_{sub}$ and diameter $d = 0.04\lambda$ was introduced along the non-radiating edge. For this purpose, we selected four positions. As shown in Fig. 8, these positions were varied from the center (Position E) to the corner of the patch (Position H). Without the blind via, the MPA worked at 2.985 GHz. Once the blind via was introduced at Position E, f_r increased from 2.98 to 3.026 GHz (41 MHz). Similarly, Position F shifted the f_r to a higher frequency but provided a lesser shift (31 MHz). Unlike the previous positions, Position G and Position H caused f_r to shift to lower values. In particular, Position H translated f_r to 2.942 GHz (a shift of 43 MHz) because of its proximity to the radiating edge.

Similar to the case of radiating edges, the central position (Position E) induced the maximum shift to higher frequencies. Furthermore, because of the symmetry of the MPA, both the non-radiating edges performed in a similar fashion. When one via was placed on either side of the non-radiating edges (i.e., for a total of two vias), a larger frequency shift could be achieved. This configuration is advantageous because it preserves the symmetry while exerting no significant influence over the directivity of the antenna. In summary, inserting a blind via along the radiating edge causes the f_r of the MPA to move to a lower value, whereas inserting two blind vias along the non-radiating edges can move f_r to a higher frequency. Consequently, the proposed technique is demonstrated to enable tuning of f_r in both directions.

B. VIA DIMENSION STUDY

Another parameter, essential to this study, is the dimensions of the via, i.e., diameter d and height H; these parameters have an influence on f_r. Note that, without the blind via, the MPA works at 2.985 GHz. To study the influence of the height of a via placed along the radiating edge, a via of $d = 0.04\lambda$ was inserted in the center position and its height was varied from $H = 0.1h_{sub}$ to $H = 0.9h_{sub}$. The central position was selected because it provides the best shift and will ease the alignment and fabrication processes. Taller vias provide a larger frequency shift in the downward direction. In particular, the height of $0.7h_{sub} - 0.9h_{sub}$ can lead to considerable shifts of f_r, whereas H < $0.7h_{sub}$ has almost no effect on f_r. As shown in Fig. 9, $H = 0.7h_{sub}$ provides a shift of 105 MHz, whereas $H = 0.9h_{sub}$ provides a larger shift of 367 MHz.

As discussed above, placing a via in this position introduces extra capacitance and thus lowers f_r. Since capacitance

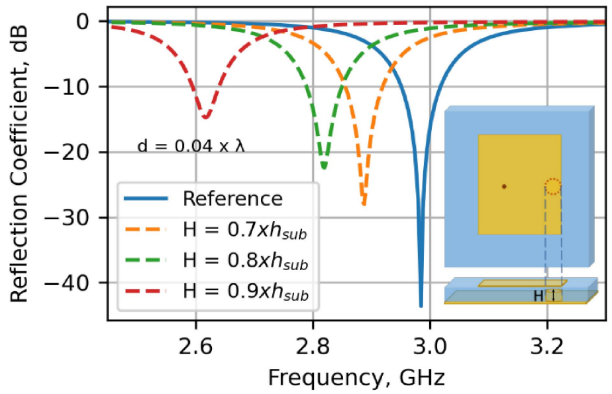

FIGURE 9. Resonant frequency shift with respect to the blind via height (radiating edge).

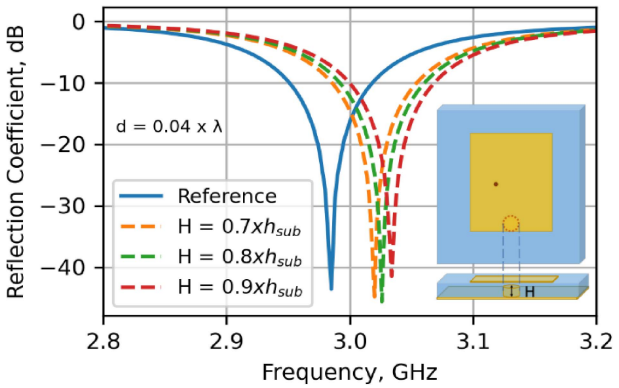

FIGURE 10. Resonant frequency shift with respect to the blind via height (non-radiating edge).

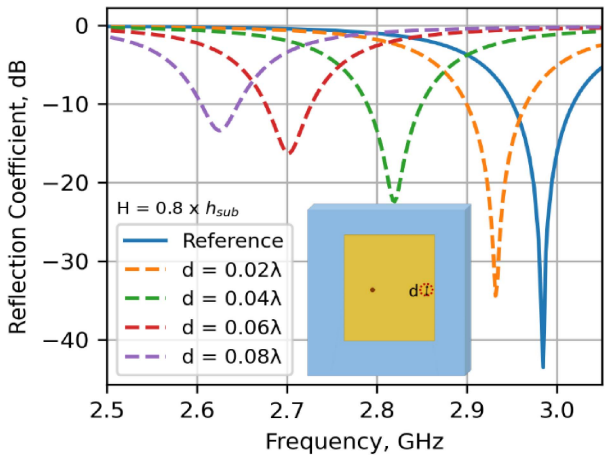

FIGURE 11. Resonant frequency shift with respect to blind via diameter (radiating edge).

is inversely proportional to the distance between two parallel plates (the patch and top surface of the via), decreasing the distance between the patch and the upper via surface, increases the introduced capacitance and induced a larger downward frequency shift.

The influence of the height of a via placed along the non-radiating edge on f_r has been studied. To evaluate this influence, a via of $d = 0.04\lambda$ was inserted into the center position of the non-radiating edge and its height was varied from $H = 0.1h_{sub}$ to $H = 0.9h_{sub}$. Generally, a taller via provides a larger shift upwards. Similar to previous case, the height of $0.7h_{sub} - 0.9h_{sub}$ can provide a considerable shift in f_r, whereas $H < 0.7h_{sub}$ has almost no effect on f_r. As shown in Fig. 10, $H = 0.9h_{sub}$ provides the largest shift (49 MHz). For the proposed technique, we chose to fix the height in order to ease the selection process of the via dimensions. We chose $H = 0.8h_{sub}$ to improve the isolation of the patch from the via.

To study the influence of the diameter of the via along the radiating edge, a via of $H = 0.8h_{sub}$ was inserted into the center position of the radiating edge and its diameter was varied from $d = 0.02\lambda$ to $d = 0.08\lambda$. In the absence of the via, the antenna worked at 2.985 GHz. As shown in Fig. 11, when a via of $d = 0.02\lambda$ is inserted, f_r shifts downwards by 53 MHz. Increasing the diameter of the via diameter causes the amount of downwards shift to increase. In particular, a shift of 359 MHz occurs when using a via with $d = 0.08\lambda$. It is known that the capacitance between two plates (the patch and via top surface) is proportional to the area of the plate overlap. Thus, increasing the via diameter provides a larger downward shift; however, too large size of via ($d > 0.1\lambda$) may cause deterioration of the antenna and significantly decrease its efficiency. According to capacitance theory, another technique by which the amount of shift may be enhanced is to increase the number of vias symmetrically along the two radiating edges; however, a greater number of vias can result in lower efficiency and a degradation of gain.

The influence of the diameter of the via placed along the non-radiating edge was studied. For this purpose, two vias of $H = 0.8h_{sub}$ were inserted in the center of two non-radiating edges and their diameters were varied between $d = 0.02\lambda$ and $d = 0.08\lambda$. This configuration was chosen to preserve symmetry while minimizing influence on antenna directivity. Without the via, the antenna works at 2.985 GHz. If vias of $d = 0.02\lambda$ are inserted, f_r increases to 3.01 GHz as shown in Fig. 12. As the diameter increases, the upwards shift also increases. For vias of $d = 0.08\lambda$, a shift of 320 MHz occurs. However, too large via may cause deterioration in antenna matching. Based on the above analysis, we conclude that d is a key parameter to control the amount of shift.

The introduction of a metallic via may lower the efficiency and gain of the antenna; as such, it is important to quantify its influence. Therefore, for the proposed technique, we conducted a study to investigate the influence of via diameter on the amount of frequency shift (in %), and antenna realized gain and total efficiency for both the downward and upward shifts.

Fig. 13(a) shows the amount of downward shift when the via is placed in the center position of the radiating edge. The radiating edge furthest from the coaxial cable was chosen in order to ease the fabrication process. The maximum

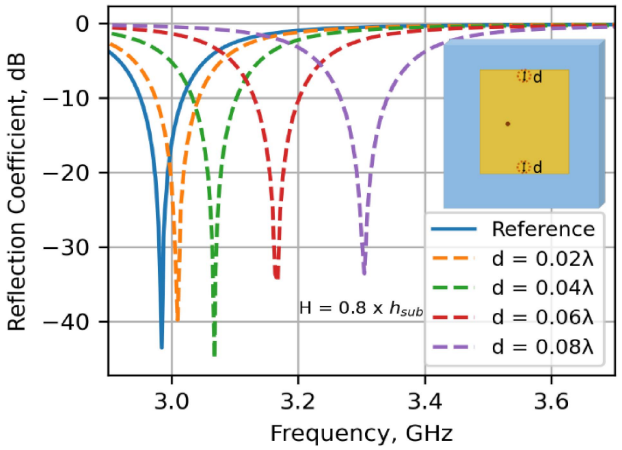

FIGURE 12. Resonant frequency shift with respect to blind via diameter (non-radiating edge).

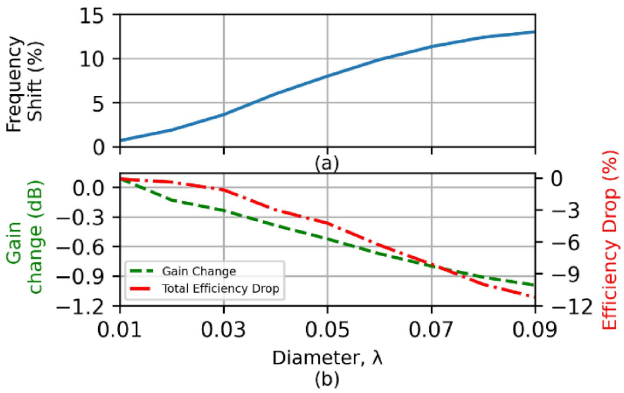

FIGURE 13. Resonant frequency shift to a lower value with one via on radiating edge. The reference antenna's maximum gain and total efficiency are 4.24 dB and 85.33%, respectively.

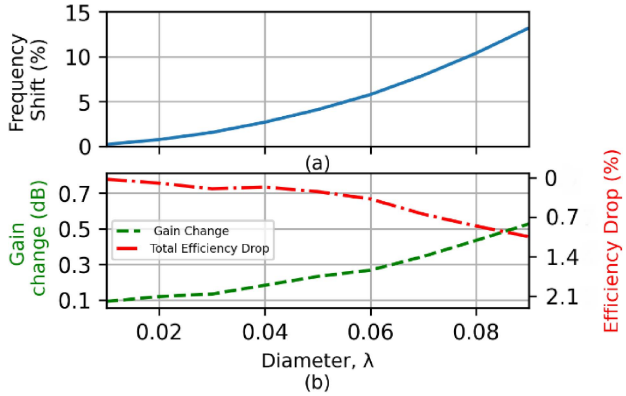

FIGURE 14. Resonant frequency shift to a higher value with two vias on the non-radiating edge. The reference antenna's maximum gain and total efficiency are 4.24 dB and 85.33%, respectively.

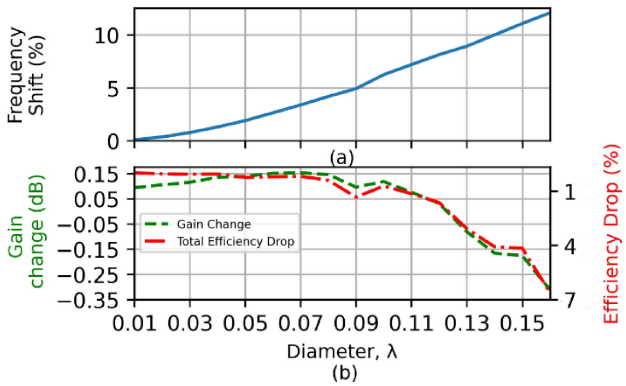

FIGURE 15. Resonant frequency shift to a higher value with one via on the non-radiating edge. The reference antenna's maximum gain and total efficiency are 4.24 dB and 85.33%, respectively.

shift is 13% with $d = 0.09\lambda$. Fig. 13(b) shows the gain and total efficiency of the antenna with the via measured at new f_r and a comparison with the reference antenna. The reference antenna's realized gain and total efficiency are 4.24 dB and 85.33%, respectively. Smaller vias ($d < 0.06\lambda$) are recommended in order to avoid large gain and a reduction in efficiency. It is possible to achieve a larger shift at the expense of gain and efficiency.

Fig. 14(a) shows the amount of upward shift (in %) with the respect to d when two vias are placed in the centers of the non-radiating edges. The maximum shift is up to 13% with $d = 0.09\lambda$. Generally, it is not recommended to use $d > 0.09\lambda$ because it worsens the reflection coefficient of the antenna. As mentioned above, this configuration is advantageous in terms of gain performance. This has also been validated by EM simulations, as shown in Fig. 14(b). Although the efficiency of the antenna is decreased, its directivity increases due to the symmetry of the via placement. Fig. 15(a) shows the amount of shift when only one via is placed. The maximum shift is up to 11% at $d = 0.15\lambda$. As shown in Fig. 15(b), in this configuration, both the gain and efficiency are almost steady up to $d = 0.11\lambda$, after which both begin to decrease.

C. GUIDELINES FOR RESONANT FREQUENCY CORRECTION TECHNIQUE UTILIZING BLIND VIAS

The frequency shift depends upon both the position and the dimensions of the via. It is important to select the correct position and dimensions of the via to achieve resonant frequency corrections resulting from material property variations. In order to facilitate this selection, we have devised guidelines for various via parameters, which are described in detail below.

To translate the resonance to lower frequencies:

1. Calculate the required frequency shift (in %) as in (1), where $f_{desired}$ is the original f_r in EM simulations and f_{actual} is the resonant frequency of the fabricated antenna different from the original f_r due to material variation:

$$\%\ shift = \frac{|f_{\text{actual}} - f_{\text{desired}}|}{f_{\text{desired}}} \times 100\ \% \tag{1}$$

2. According to Fig. 13(a), choose the via diameter (d) for the calculated shift. For example, if a shift of 7.5% is desired, select a via diameter of $d = 0.05\lambda$.

TABLE 1. Gain performance.

	Simulated gain, dB	Fabricated gain, dB	Post-fabricated gain, dB
Non-radiating edge	5.26	5.28	5
Radiating Edge	5.19	5.27	4.86

3. Insert the via into the central position of the radiating edge.

To translate the resonance frequency to higher values:

1. Calculate the required frequency shift (in %) as in (1).
2. According to Fig. 14(a), choose the via diameter (d) for the desired frequency shift. For example, if a shift of 2.5% is desired, select a via diameter of $d = 0.04\lambda$.
3. Insert the first via at the central position of the non-radiating edge. Insert the second via at the central position of opposite non-radiating edge.
4. If only one via is preferred, select the via diameter according to Fig. 15(a) and insert this via at the central position of the non-radiating edge.

IV. VALIDATION OF PROPOSED TECHNIQUE THROUGH EXPERIMENTATION

To validate the proposed technique, a patch antenna working at 2.98 GHz was fabricated as shown in Fig. 16. A dielectric layer of ABS with a length of 56 mm, a width of 50 mm a height of 1.5 mm, an εr of 3, and a loss tangent of 0.0046 is printed using a 3D Raise Printer, whereas the conductor layers are applied using a silver paste. Due to the permittivity variation, the antenna operates at 3.036 GHz. The following steps are then taken according to the guidelines presented in Section III:

1. As per (1), a percentage shift of 1.75% toward a lower value is required.
2. To shift the resonance to a lower value, $d = 0.02\lambda$ was chosen according to Fig. 13(a). The radiating edge farthest from the coaxial cable was selected such that the feed point does not interfere with the fabrication process.
3. The via is inserted at the central position of the chosen radiating edge. The via hole is cut using a laser VLS 3.50 10.6 uμ, filled with a silver paste, and dried in the oven. Note that it is advised to drill by an accurate method to reach the necessary resonant frequency shift.

As shown in Fig. 17, the antenna f_r is corrected from 3.036 GHz to 2.99 GHz. The corrected f_r matches the desired simulated resonant frequency. Its error is 0.33% due to the quality of the laser cut. The Gaussian distribution of the laser light entails that the laser cuts the via hole in the form of a cylinder with various imperfections at its surfaces and at the edges of the hole. As shown in Fig. 19(a), the post-fabricated antenna has a gain of 4.87 dB compared to 5.27 dB in previously fabricated antenna. The antenna radiation pattern is not altered by the introduction of the via.

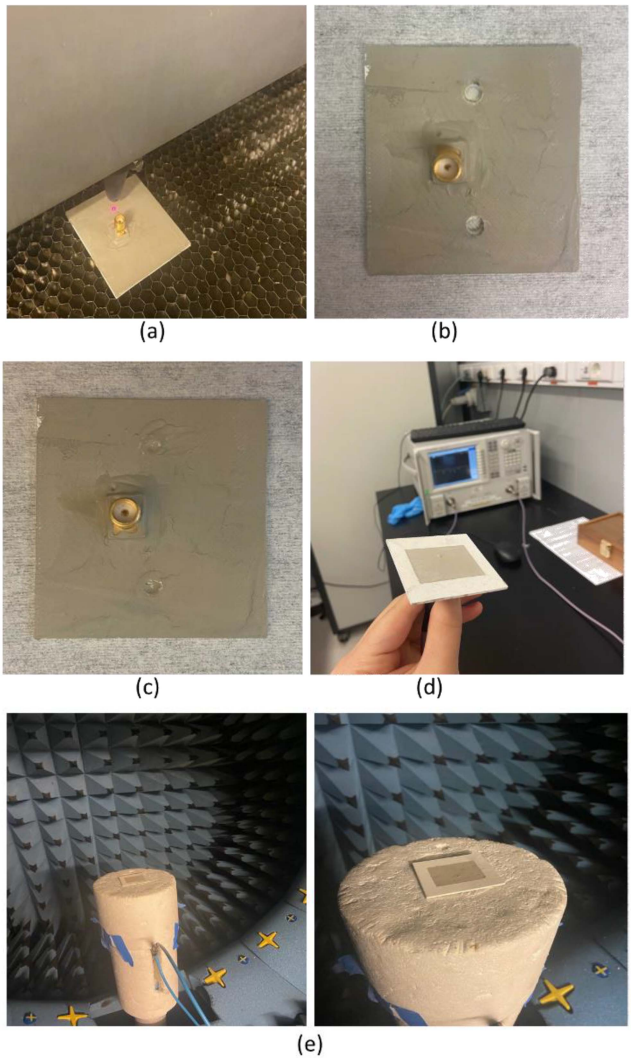

FIGURE 16. (a) Cutting the via holes using the laser. (b) Antenna ground plane with via holes. (c) Antenna ground plane featuring a blind via filled with conductive silver paste. (d) VNA measurements. (e) Measurements in anechoic chamber.

To validate the translation to a higher frequency, a patch antenna working at 3.04 GHz was fabricated. Similarly, a dielectric layer with a height of 1.5 mm and an indicated ε_r of 3 was printed using a 3D Raise Printer. The patch and ground plane were applied using the silver paste. The desired f_r is 3.11 GHz. To compensate for material variation, guidelines suggest that the resonance should be shifted toward a higher frequency. The following steps were therefore taken according to guidelines presented in Section III.

1. The required percentage shift was approximately 2.5% as per (1).
2. Two blind vias with a diameter of 0.04λ were chosen according to Fig. 14(a).
3. Two holes in the central positions of the non-radiating edges were drilled using the laser. They were subsequently filled with a conductive silver paste and dried using an oven.

These vias translated the resonance position from 3.04 GHz to 3.1 GHz, as shown in Fig. 18. The corrected

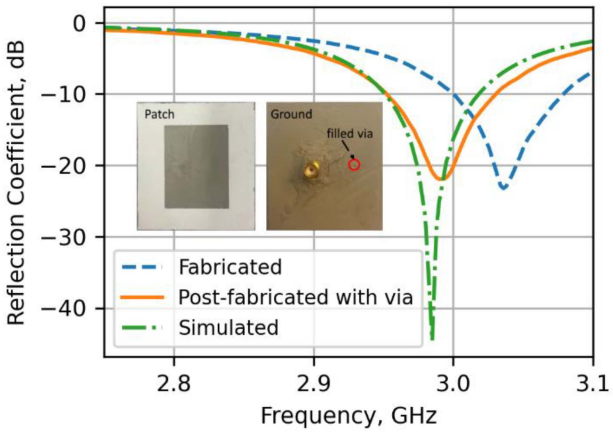

FIGURE 17. Translation of the resonance position to lower frequencies.

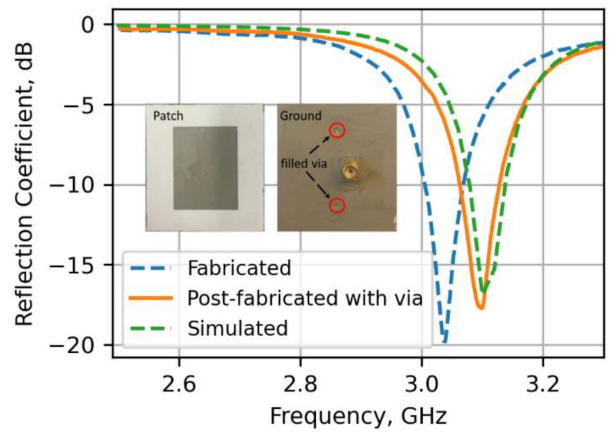

FIGURE 18. Translation of the resonance position to higher frequencies.

f_r matches the desired simulated resonant frequency. As shown in Fig. 19(b), the post-fabricated antenna gain with two vias of $d = 0.04\lambda$ is 5 dB compared to 5.28 dB in the previously fabricated antenna. The commercial silver paste was dried below the recommended temperature in order to avoid damaging the dielectric layer. This led to lower conductivity and, subsequently, lower efficiency and gain, than expected. The radiation pattern was not altered by the introduction of the via.

V. CONCLUSION

This paper has presented a post-fabrication technique to correct for the f_r of a 3D-printed rectangular MPA. The proposed technique utilizes either a single blind via or an array of vias in a 3D-printed substrate to regulate the f_r of the antenna at a desired value. This technique can be used to move the resonance position by 13% in both the directions. Although a shift above 13% is possible, it is achieved at the expense of gain and efficiency. A complete set of guidelines has been provided for selecting the via dimensions and position to achieve the desired frequency shift. Subsequently, the proposed technique is validated through experimentation. The corrected f_r of the fabricated

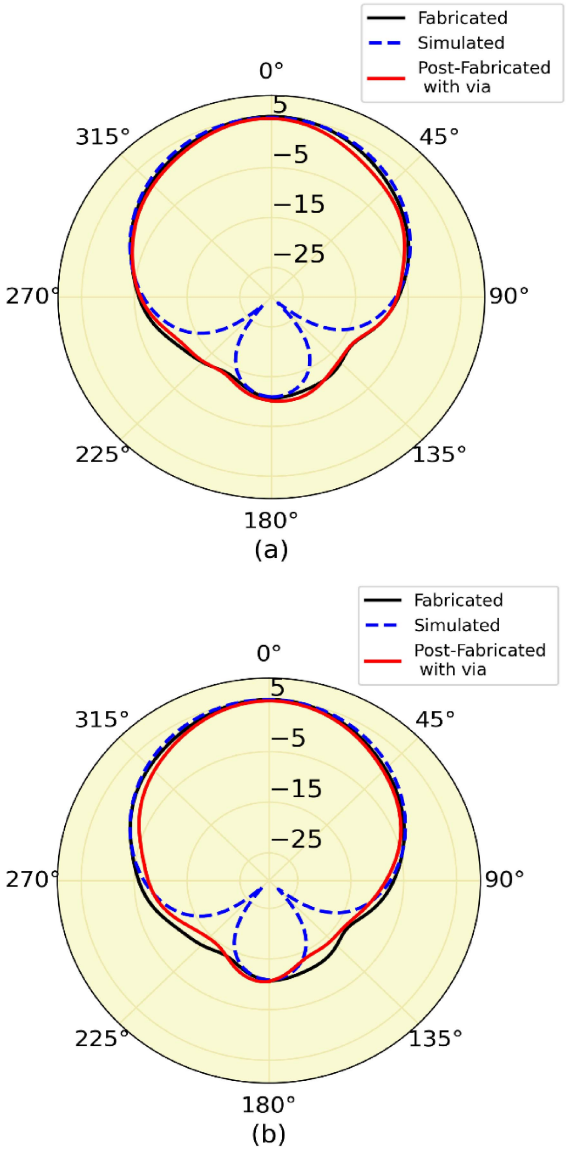

FIGURE 19. Antenna gain with (a) one via along the radiating edge and (b) two vias along non-radiating edges.

antennas matches the expected resonant frequencies with minor variations, which may be caused by imperfections attributed to the laser cut. In future research, the applicability of the technique to rigid substrates (like FR4) should be studied.

REFERENCES

[1] D. Savastano, "Flexible and printed electronics are becoming more mainstream," *Printed Electron.*, vol. 9, no. 1, pp. 11–13, 2021.
[2] Z. Y. Lopez, Z. Akhter, and A. Shamim, "3D printed RFID tag antenna miniaturized through volumetric folding and slow-wave structures," *IEEE J. Radio Freq. Identification*, vol. 6, pp. 164–175, 2022.
[3] F. Wei, J. W. Hao, L. Xu, and X. Shi, "A circularly polarized 3-D printed dielectric transmitarray antenna at millimeter-wave band," *IEEE Antennas Wireless Propag. Lett.*, vol. 20, no. 7, pp. 1264–1268, Jul. 2021, doi: 10.1109/LAWP.2021.3077290.
[4] M. F. Farooqui, M. A. Karimi, K. N. Salama, and A. Shamim, "3D-printed disposable wireless sensors with integrated microelectronics for large area environmental monitoring," *Adv. Mater. Technol.*, vol. 2, no. 8, 2017, Art. no. 1700051.

[5] M. F. Farooqui and A. Kishk, "3-D-printed tunable circularly polarized microstrip patch antenna," *IEEE Antennas Wireless Propag. Lett.*, vol. 18, no. 7, pp. 1429–1432, Jul. 2019, doi: 10.1109/LAWP.2019.2919255.

[6] Z. Su, K. Klionovski, R. M. Bilal, and A. Shamim, "A dual band additively manufactured 3-D antenna on package with near-isotropic radiation pattern," *IEEE Trans. Antennas Propag.*, vol. 66, no. 7, pp. 3295–3305, Jul. 2018, doi: 10.1109/TAP.2018.2823729.

[7] K. Liu, C. Zhao, S.-W. Qu, Y. Chen, J. Hu, and S. Yang, "A 3-D-printed multibeam spherical lens antenna with ultrawide-angle coverage," *IEEE Antennas Wireless Propag. Lett.*, vol. 20, no. 3, pp. 411–415, Mar. 2021, doi: 10.1109/LAWP.2021.3054042

[8] G. McKerricher, D. Titterington, and A. Shamim, "A fully inkjet-printed 3-D honeycomb-inspired patch antenna," *IEEE Antennas Wireless Propag. Lett.*, vol. 15, pp. 544–547, 2016, doi: 10.1109/LAWP.2015.2457492.

[9] Y. Li et al., "3-D printed high-gain wideband waveguide fed horn antenna arrays for millimeter-wave applications," *IEEE Trans. Antennas Propag.*, vol. 67, no. 5, pp. 2868–2877, May 2019, doi: 10.1109/TAP.2019.2899008.

[10] M. B. Arboleda, K. Klionovski, S. Zhen, and A. Shamim, "Orientation aware intelligent 3-D cubic antenna system with automated radiation pattern reconfigurability," *IEEE Open J. Antennas Propag.*, vol. 3, pp. 812–823, 2022, doi: 10.1109/OJAP.2022.3190218.

[11] C. Wang, J. Wu, and Y. X. Guo, "A 3-D-printed wideband circularly polarized parallel-plate luneburg lens antenna," *IEEE Trans. Antennas Propag.*, vol. 68, no. 6, pp. 4944–4949, Jun. 2020, doi: 10.1109/TAP.2019.2955222.

[12] H. Liao, Q. Zhang, M. A. Karimi, Y.-H. Kuo, N. Mishra, and A. Shamim, "An additively manufactured 3-D antenna-in-package with quasi-isotropic radiation for marine animals monitoring system," *IEEE Antennas Wireless Propag. Lett.*, vol. 18, no. 11, pp. 2384–2388, May 2020, doi: 10.1109/LAWP.2019.2937507.

[13] X. Zhang et al., "3-D printed Swastika-shaped ultrabroadband water-based microwave absorber," *IEEE Antennas Wireless Propag. Lett.*, vol. 19, no. 5, pp. 821–825, May 2020.

[14] S. Ghosh and S. Lim, "Perforated lightweight broadband metamaterial absorber based on 3-D printed honeycomb," *IEEE Antennas Wireless Propag. Lett.*, vol. 17, no. 12, pp. 2379–2383, Dec. 2018, doi: 10.1109/LAWP.2018.2876023.

[15] K. Lomakin et al., "3D printed E-band hybrid coupler," *IEEE Microwave Wireless Compon. Lett.*, vol. 29, no. 9, pp. 580–582, Sep. 2019.

[16] A. Vallecchi, D. Cadman, W. G. Whittow, J. Vardaxoglou, E. Shamonina, and C. J. Stevens, "3-D printed bandpass filters with coupled vertically extruded split ring resonators," *IEEE Trans. Microwave Theory Techn.*, vol. 67, no. 11, pp. 4341–4352, Nov. 2019, doi: 10.1109/TMTT.2019.2934456.

[17] S. S. Cho, S. H. Yoon, and I. P. Hong, "Design of three-dimensional frequency selective structure with replaceable unit structures using a 3-D printing technique," *IEEE Antennas Wireless Propag. Lett.*, vol. 17, no. 11, pp. 2041–2045, Nov. 2018, doi: 10.1109/LAWP.2018.2871175.

[18] E. Laplanche et al., "A ku-band diplexer based on 3dB directional couplers made by plastic additive manufacturing," in *Proc. 47th Eur. Microwave Conf. (EuMC)*, 2017, pp. 428–431, doi: 10.23919/EuMC.2017.8230881.

[19] Y. Li, L. Ge, M. Chen, Z. Zhang, Z. Li, and J. Wang, "Multibeam 3-D-printed luneburg lens fed by magnetoelectric dipole antennas for millimeter-wave MIMO applications," *IEEE Trans. Antennas Propag.*, vol. 67, no. 5, pp. 2923–2933, May 2019, doi: 10.1109/TAP.2019.2899013.

[20] G. B. Wu, Y. S. Zeng, K. F. Chan, S. W. Qu, and C. H. Chan, "3-D printed circularly polarized modified fresnel lens operating at terahertz frequencies," *IEEE Trans. Antennas Propag.*, vol. 67, no. 7, pp. 4429–4437, Jul. 2019, doi: 10.1109/TAP.2019.2908110.

[21] H. Giddens, A. S. Andy, and Y. Hao, "Multimaterial 3-D printed compressed luneburg lens for mm-Wave beam steering," *IEEE Antennas Wireless Propag. Lett.*, vol. 20, no. 11, pp. 2166–2170, Nov. 2021, doi: 10.1109/LAWP.2021.3109591.

[22] J. C. Balzer, M. Weidenbach, S. F. Busch, and M. Koch, "3D printed waveguides for 120 GHz," in *Proc. German Microwave Conf. (GeMiC)*, 2016, pp. 1–3, doi: 10.1109/GEMIC.2016.7461540.

[23] J. Persad and S. Rocke, "A survey of 3D printing technologies as applied to printed electronics," *IEEE Access*, vol. 10, pp. 27289–27319, 2022, doi: 10.1109/ACCESS.2022.3157833.

[24] J. Huang, S. J. Chen, Z. Xue, W. Withayachumnankul, and C. Fumeaux, "Wideband endfire 3-D-printed dielectric antenna with designable permittivity," *IEEE Antennas Wireless Propag. Lett.*, vol. 17, no. 11, pp. 2085–2089, Nov. 2018, doi: 10.1109/LAWP.2018.2857497.

[25] C. Tomassoni, R. Bahr, M. Tentzeris, M. Bozzi, and L. Perregrini, "3D printed substrate integrated waveguide filters with locally controlled dielectric permittivity," in *Proc. 46th Eur. Microwave Conf. (EuMC)*, 2016, pp. 253–256, doi: 10.1109/EuMC.2016.7824326.

[26] S. Moscato et al., "Infill dependent 3D-printed material based on NinjaFlex Filament for antenna applications," *IEEE Antennas Wireless Propag. Lett.*, vol. 15, pp. 1506–1509, 2016.

[27] H. Saleh, H. Tortel, C. Leroux, A. Coudreuse, A. Litman, and J.-M. Geffrin, "Approach to control permittivity and shape of centimeter-sized additive manufactured objects: Application to microwave scattering experiments," *IEEE Trans. Antennas Propag.*, vol. 69, no. 2, pp. 983–991, Feb. 2021, doi: 10.1109/TAP.2020.3016159.

[28] E. Marquez-Segura, S.-H. Shin, A. Dawood, N. M. Ridler, and S. Lucyszyn, "Microwave characterization of conductive PLA and its application to a 12 to 18 GHz 3-D printed rotary vane attenuator," *IEEE Access*, vol. 9, pp. 84327–84343, 2021. [Online]. Available: https://www.rogerscorp.com/advanced-electronics-solutions/rt-duroid-laminates/rt-duroid-5880-laminates

[29] Rogers Corporation. "RO4000 series high frequency circuit materials." [Online]. Available: https://www.rogerscorp.com/advanced-electronics-solutions/ro4000-series-laminates/ro4003c-laminates

[30] Taconic. "TLC Low Cost RF Subtsrate." [Online]. Available: http://www.taconic.co.kr/download/TLC.pdf

[31] J. Tang, R. O. Ouedraogo, E. J. Rothwell, A. R. Diaz, and K. Fuchi, "A continuously tunable miniaturized patch antenna," *IEEE Antennas Wireless Propag. Lett.*, vol. 13, pp. 1080–1083, 2014, doi: 10.1109/LAWP.2014.2329332.

[32] A. Singh and C. E. Saavedra, "Fluidic stub-loaded patch antenna for frequency-tunable polarization reconfiguration," *IEEE Open J. Antennas Propag.*, vol. 2, pp. 362–369, 2021, doi: 10.1109/OJAP.2021.3063281.

[33] S. Wang, L. Zhu, and W. Wu, "A novel frequency-reconfigurable patch antenna using low-loss transformer oil," *IEEE Trans. Antennas Propag.*, vol. 65, no. 12, pp. 7316–7321, Dec. 2017, doi: 10.1109/TAP.2017.2758204.

[34] A. Shamim, J. R. Bray, N. Hojjat, and L. Roy, "Ferrite LTCC-based antennas for tunable SoP applications," *IEEE Trans. Compd. Packag. Manuf. Technol.*, vol. 1, no. 7, pp. 999–1006, Jul. 2011, doi: 10.1109/TCPMT.2011.2143411.

[35] F. A. Ghaffar, J. R. Bray, and A. Shamim, "Theory and design of a tunable antenna on a partially magnetized ferrite LTCC substrate," *IEEE Trans. Antennas Propag.*, vol. 62, no. 3, pp. 1238–1245, Mar. 2014, doi: 10.1109/TAP.2013.2295833.

[36] J. L. Salazar-Cerreno, Z. Qamar, S. Saeedi, B. Weng, and H. S. Sigmarsson, "Frequency agile microstrip patch antenna using an anisotropic artificial dielectric layer (AADL): Modeling and design," *IEEE Access*, vol. 8, pp. 6398–6406, 2020, doi: 10.1109/ACCESS.2019.2962160.

[37] A. K. Bordoloi, P. Borah, S. Bhattacharyya, and N. S. Bhattacharyya, "A novel approach for post fabrication fine tuning and matching of microstrip patch antenna using adjustable air pocket in substrate layer," in *Proc. Loughborough Antennas Propag. Conf.*, 2011, pp. 1–3, doi: 10.1109/LAPC.2011.6114026.

[38] D. Schaubert, F. Farrar, A. Sindoris, and S. Hayes, "Frequency agile microstrip antennas," in *Proc. Antennas Propag. Soc. Int. Symp.*, 1980, pp. 601–604, doi: 10.1109/APS.1980.1148248.

[39] D. Schaubert, F. Farrar, A. Sindoris, and S. Hayes, "Microstrip antennas with frequency agility and polarization diversity," *IEEE Trans. Antennas Propag.*, vol. 29, no. 1, pp. 118–123, Jan. 1981, doi: 10.1109/TAP.1981.1142546.

[40] G. P. Gao, C. Yang, B. Hu, R. F. Zhang, and S. F. Wang, "A wide-bandwidth wearable all-textile PIFA with dual resonance modes for 5 GHz WLAN applications," *IEEE Trans. Antennas Propag.*, vol. 67, no. 6, pp. 4206–4211, Jun. 2019, doi: 10.1109/TAP.2019.2905976.

[41] K. D. Xu, H. Xu, Y. Liu, J. Li, and Q. H. Liu, "Microstrip patch antennas with multiple parasitic patches and shorting vias for bandwidth enhancement," *IEEE Access*, vol. 6, pp. 11624–11633, 2018, doi: 10.1109/ACCESS.2018.2794962.

[42] D. L. Sengupta, "Transmission line model analysis of rectangular patch antennas," *Electromagnetics*, vol. 4, no. 4, pp. 355–376, 1984.

[43] D. L. Sengupta, "Resonant frequency of a tunable rectangular patch antenna," *Electron. Lett.*, vol. 20, pp. 614–615, Apr. 1984.
[44] K. Güney, "Resonant frequency of a tunable rectangular microstrip patch antenna," *Microwave Opt. Technol. Lett.*, vol. 7, no. 12, pp. 581–585, 1994.
[45] W. F. Richards and Y. T. Lo, "Theoretical and experimental investigation of a microstrip radiator with multiple lumped linear loads," *Electromagnetics*, vol. 3, nos. 3–4, pp. 371–385, 1983.
[46] S. S. Zhong and Y. T. Lo, "Single-element rectangular microstrip antenna for dual-frequency operation," *Electron. Lett.*, vol. 19, no. 8, p. 298, 1983.
[47] Ultimaker. "Ultimaker S3." [Online]. Available: https://ultimaker.com/3d-printers/ultimaker-s3
[48] Flashforge 3D Printer. "Creator Pro." [Online]. Available: https://www.flashforgeshop.com/product/flashforge-creator-pro-2-3d-printer-independent-dual-extruder?cID=21
[49] Raise3D. "3D raise printer." Accessed: Nov. 21, 2022. [Online]. Available: https://www.raise3d.com/pro3-series/
[50] C. A. Balanis, *Microstrip Antennas Antenna Theory: Analysis and Design*, 3rd ed. Hoboken, NJ, USA: Wiley, 2005, pp. 811–876.

ZERE IMAN received the bachelor's degree in electrical engineering from Nazarbayev University, Astana, Kazakhstan, in 2020, and the M.S. degree in electrical and computer engineering from the King Abdullah University of Science and Technology, Saudi Arabia, in 2022, where she is currently pursuing the Ph.D. degree.

Her research interests include 3-D printing, inkjet-printing, on-chip antennas, and millimeter-wave antennas.

ZUBAIR AKHTER (Member, IEEE) received the bachelor's degree in electronics and instrumentation engineering from Anand Engineering College, Agra, India, in 2008, the M.Tech. degree in RF and microwave engineering from the Indian Institute of Technology Roorkee, Roorkee, India, in 2011, and the Ph.D. degree in electrical engineering from the Indian Institute of Technology Kanpur, Kanpur, India, in 2018, with a focus on microwave imaging, sensing, and nondestructive testing of materials, through-wall imaging, and ultra-wideband antennas.

He is currently associated with the King Abdullah University of Science and Technology (KAUST), Saudi Arabia, as a Postdoctoral Fellow, where he worked with the world's top funding agencies, such as Lockheed Martin Corporation, Ericsson, SABIC, and Aramco for solving the applied industrial challenges. His research for Lockheed Martin on "ultra-thin, dual-mode wideband circular microstrip antennas for UAVs" was featured by the IEEE OPEN JOURNAL OF ANTENNAS AND PROPAGATION. Before joining KAUST, he was associated with Abu Dhabi National Oil Company Gas Research Center as a Research Engineer. He is an Inventor of 6 U.S. patents and has given 12 invited talks at various internationally recognized forums/institutions. He has authored/coauthored over 60 international publications published in top-notch peer-reviewed journals, such as IEEE TRANSACTIONS ON MICROWAVE THEORY AND TECHNIQUES, IEEE TRANSACTIONS ON ANTENNAS AND PROPAGATION, IEEE TRANSACTIONS ON INSTRUMENTATION AND MEASUREMENT, IEEE SENSORS JOURNAL, and various admired international conferences. His current research interests are in microwave sensing, non-destructive testing for the oil and gas industry, printed-flexible electronics, printed transparent antennas, chipless RFID sensing, IoT applications, and ultra-thin UAV antennas. He is a recipient of the Early Career Researcher Teaching Award from the Office of the Provost in collaboration with the Office of Vice President (Research) at King Abdullah University of Science and Technology. He is the Founding Chair of the IEEE Antennas and Propagation Student Branch Chapter, Indian Institute of Technology Kanpur. He is currently an editorial board member in frontiers wearable electronics and served as a member of the Technical Program Committee in IMaRC-2021 and MAPCON-2022.

YIYANG YU (Graduate Student Member, IEEE) received the B.Eng. degree in electromagnetics and wireless technology from the University of Electronic Science and Technology of China, China, in 2019, and the M.S. degree in electrical and computer engineering from the King Abdullah University of Science and Technology, Saudi Arabia, in 2021, where he is currently pursuing the Ph.D. degree.

His current research interests include millimeter-wave antennas, on-chip antennas, artificial magnetic conductors, and electrically small antennas.

ATIF SHAMIM (Senior Member, IEEE) received the M.S. and Ph.D. degrees in electrical engineering from Carleton University, Ottawa, ON, Canada, in 2004 and 2009, respectively.

He was an NSERC Alexander Graham Bell Graduate Scholar with Carleton University from 2007 to 2009, an NSERC Postdoctoral Fellow with Royal Military College Canada from 2009 to 2010, and the King Abdullah University of Science and Technology (KAUST), Thuwal, Saudi Arabia. In August 2010, he joined the Electrical Engineering Program, KAUST, where he is currently a Professor and the Principal Investigator of the IMPACT Lab. He was an invited Researcher with VTT Micro-Modules Research Center, Oulu, Finland, in 2006. He is an author of one book, three book chapters, and 250 publications; an inventor on 30 patents; and has given 70 invited talks at various international forums. His research interests include innovative antenna designs and their integration strategies with circuits and sensors for flexible and wearable wireless sensing systems through a combination of CMOS and additive manufacturing technologies. He was the recipient of Best Paper Awards in IEEE IMS 2016, IEEE MECAP 2016, IEEE EuWiT 2008; the First Prize in the IEEE IMS 2019 3MT competition; the Finalist/Honorable Mention Prizes in IEEE APS Design Competition 2020, IEEE APS 2005, IEEE IMS 2014, and IEEE IMS 2017 (3MT competition); and R. W. P. King IEEE Award for journal papers in IEEE TAP 2017 and 2020. He was given the Ottawa Centre of Research Innovation (OCRI) Researcher of the Year Award, Canada, in 2008. His work on wireless dosimeter won the ITAC SMC Award at Canadian Microelectronics TEXPO in 2007. He also was the recipient of numerous business-related awards, including 1st Prize in Canada's National Business Plan Competition and the OCRI Entrepreneur of the Year Award in 2010 and the Kings Prize for the best innovation of the year in 2018 for his work on sensors for the oil industry. He served on the editorial board of IEEE TRANSACTIONS ON ANTENNAS AND PROPAGATION from 2013 to 2019, and as the Guest Editor for IEEE AWPL Special issue in 2019. He is currently an Associate Editor for IEEE JOURNAL OF ELECTROMAGNETICS, RF AND MICROWAVES IN MEDICINE AND BIOLOGY. He was selected as the Distinguished Lecturer for AP-S from 2022 to 2024. He is a Member of the IEEE APS Measurements Committee and the IEEE MTT Microwave Control Techniques Committee, founded the First IEEE AP/MTT Chapter in Saudi Arabia, in 2013.